Developing Halogen-Free Polymer Donor for Efficient Nonfullerene Organic Solar Cells by Addition of Highly Electron-Deficient Diketopyrrolopyrrole Unit

Ji, Jingjing; Xie, Jiaqi; Tang, Junhui; Zheng, Kaibo; Liang, Ziqi

Published in:
Solar RRL

Link to article, DOI:
10.1002/solr.202100142

Publication date:
2021

Document Version
Peer reviewed version

DOI: 10.1002/advs.2021xxxxx
Article type: Full Paper

Developing Halogen-Free Polymer Donor for Efficient Nonfullerene Organic Solar Cells by Addition of Highly Electron-Deficient Diketopyrrolopyrrole Unit

Jingjing Ji,[1] Jiaqi Xie,[1] Junhui Tang,[1] Kaibo Zheng,[2,3] and Ziqi Liang[1*]*

[*][1]Prof. Z. Liang, J. Ji, J. Xie, J. Tang
Department of Materials Science
Fudan University
Shanghai 200433, China
Email: zqliang@fudan.edu.cn

[*][2]Prof. K. Zheng
Department of Chemistry
Technical University of Denmark
DK-2800 Kongens Lyngby, Denmark
Email: kzheng@kemi.dtu.dk

[3]Dr. K. Zheng
Department of Chemical Physics and NanoLund
Lund University
P.O. Box 124, 22100 Lund, Sweden

Keywords: halogen-free, polymer donor, diketopyrrolopyrrole, nonfullerene acceptor, organic solar cells

ABSTRACT: High-performance polymer donors when paired with nonfullerene acceptors are mainly limited to flanking halogenated benzodithiophene (BDT)-based π-conjugated copolymers, which however involve the complex synthetic procedures. Herein, we developed a series of halogen-free polymer donors that link BDT moiety with two highly electron-deficient benzodithiophene-dione (BDD) and diketopyrrolopyrrole (DPP) units with various molar ratios.

Compared with the benchmark PBDB-T donor containing BDD unit, additional incorporation of stronger electron-negative DPP unit markedly lowers frontier molecular orbital levels and extends optical absorption, potentially leading to simultaneously enhanced V_{OC} and J_{SC} in organic solar cells.

A remarkable PCE of 10.28% is thus obtained in the optimal **P75** (BDD : DPP = 3 : 1 mol%) and Y6 blend cells in comparison to the reference PBDB-T:Y6 (9.20%). A slight addition of $PC_{71}BM$ into the blend is found to further generate finer phase-separated domains and thus boost the best efficiency up to 12.20%. The subtly critical roles of $PC_{71}BM$ are determined by transient absorption measurements on both thin film and in-situ devices to be the prolonged free charge carrier lifetime and the shallow charge-transfer states, which enhances J_{SC} and FF in device, respectively.

1. Introduction

In recent years, bulk-heterojunction (BHJ) organic solar cells (OSCs) have taken a leap forward based on polymer donors and acceptor–donor–acceptor (A–D–A) type non-fullerene acceptors (NFAs).[1–16] More recently, Y-system NFAs-based single-junction OSCs (denoted as NF-OSCs as follows) have demonstrated the power conversion efficiencies (PCEs) of approaching 18%,[17–27] showing a great potential toward future commercialization. However, matching polymer donors with high-performance NFAs are reported thus far to mostly fall within those benzodithiophene (BDT)-based polymer donors that are flanked with electronegative halogen atoms such as fluorine (F) and chlorine (Cl), representative of PM6, i.e., poly[1-(5-(4,8-bis(5-(2-ethylhexyl)-4-fluorothiophen-2-yl)benzo[1,2-b:4,5-b']dithiophen-2-yl)thiophen-2-yl)-5,7-bis(2-ethylhexyl)-3-(thiophen-2-yl)-4H,8H-benzo[1,2-c:4,5-c']dithiophene-4,8-dione] bearing –F side-group.[14,22,28–33] The halogenation of BDT unit in polymer donors allows to tune π-electron property to effectively enhance intermolecular packing and crystallinity as well as downshift the highest occupied molecular orbital (HOMO) energy level to increase open-circuit voltage (V_{OC}) of the resulting OSCs.[34–39] Besides, many noncovalent Coulombic interactions exist for halogen atoms—such as F···H and F···S and so on—which benefit the enhancement of π-backbone planarity,[38,41] compared to that of the halogenated-free donor polymers. Such a halogenation, however, requires complicated synthetic

steps, in particular for fluorination, and renders additional barriers for large-scale commercialization.[34,42] Therefore, it is desirable to develop halogen-free polymer donors via cost-effective synthetic routes to match NFAs and obtain comparably high photovoltaic performance.

As an alternative route to halogenation, it is highly feasible to incorporate a third unit with stronger electron-deficient property in the main chain by using random copolymerization. Diketopyrrolopyrrole (DPP) seems such a suitable third-component unit due to its accessible synthetic procedures and precise control of the polymer processability by alkylation of side chains at two *N*-positions. Arguably, the DPP moiety features highly planar π-backbone and large crystallinity, leading to strong optical absorption, while its exceptional electron-withdrawing capability enables to deepen the lowest unoccupied molecular orbital (LUMO) energy level and result in a narrower optical bandgap (E_g) in polymer donors,[43,45] both of which aid to improve light harvesting and carrier transport. However, the intrinsic drawback of high-lying HOMO level of DPP can be neglected by such a slight incorporation of DPP content in the resultant terpolymer donors.[46]

In this study, we synthesized a series of halogen-free polymer donors by incorporation of DPP moiety into the paradigm π-backbone of donor that consists of electron-rich BDT and electron-poor BDD units using Stille coupling ternary polymerization. An optimal polymer donor **P75** bearing 75 mol% BDD moiety presents lower E_g (~1.4 eV), broader absorption range (up to ~900 nm), and lower HOMO (–5.43 eV) / LUMO (–4.01 eV) energy levels than PBDB-T, i.e., poly[1-(5-(4,8-bis(5-(2-ethylhexyl)thiophen-2-yl)benzo[1,2-b:4,5-b']dithiophen-2-yl)thiophen-2-yl)-5,7-bis(2-ethylhexyl)-3-(thiophen-2-yl)-4H,8H-benzo[1,2-c:4,5c'] dithiophene-4,8-dione] without DPP moiety. When paired with Y6 acceptor, the **P75** based OSCs delivered a higher PCE of 10.28% than the PBDB-T:Y6 based device (9.2%). Upon addition of $PC_{71}BM$ acceptor, the resulting ternary **P75**:Y6:$PC_{71}BM$ based cells with an optimal ratio of 1:1.4:0.1 (wt%) achieved an impressive PCE of 12.20%. The mechanism of device enhancement is in-depth investigated by transient absorption (TA) studies on both blend thin films and working devices. The results suggest that efficient sub-picosecond photo-

induced charge transfer at D/A interfaces appears in **P75** based binary devices and subsequently the charge carrier separation and transport dynamics can be further improved by $PC_{71}BM$ addition, which enhances the electron transport and weakens the local dielectric screening, leading to the prolonged free charge carrier lifetime and shallow charge-transfer (CT) states, respectively.

2. Results and Discussion

In this work, we synthesized a series of halogen-free polymer donors by a Stille coupling reaction, in which a BDT donor moiety is copolymerized with both DPP and BDD units at a molar ratio of DPP:BDD from 1, 3:1, 1:1, 1:3 to 1. The corresponding photovoltaic devices with Y6 acceptor become gradually worse in performance with the increasing DPP ratio as seen in Table S1 in the Supporting Information (SI), which is likely caused by the deepening LUMO energy levels of donor polymer leading to a mismatch with Y6. Among them, a terpolymer donor containing 75 mol% BDD, named **P75**, shows the best photovoltaic performance in these polymers. Hence the following discussion will center on **P75** and a comparison with the reference PBDB–T and PM6 with fluorine (–F) side-group. The molecular structures, detailed synthetic procedures and elemental analysis of **P75** and PBDB–T are described in **Figure 1**a and Scheme S1 in SI, respectively. Both of them afford good solubility in chloroform (CF) and chlorobenzene (CB) solution at room temperature. Meanwhile, these two polymers exhibit high thermal stability with a decomposition temperature (T_d) over 420 °C. And there are no obvious thermal transitions by their differential scanning calorimetry curves (DSC) (Figure S1). In addition, the number-averaged molecular weight (M_n) and polydispersity index (PDI) are also comparable, that is, 35.11 kDa / 1.46 and 26.93 kDa / 1.51 for **P75** and PBDB–T, respectively, which minimizes the impact of molecular weight on the performance.[47]

The main absorption peaks of **P75**, PBDB–T and PM6 in thin films are similar as shown in Figure S2a, all ranging from 500–700 nm as a result of intramolecular charge transfer from an

electron-donating BDT unit to an electron-withdrawing BDD unit. In contrast to PBDB–T and PM6, an additional shoulder peak of **P75** locates at 750 nm originating from the stronger electron-poor DPP unit, suggesting halogen-free polymer donor can afford broader light absorption for sunlight harvesting. In addition, comparing the optical absorption spectra of **P75** and PBDB-T in both solution and thin film, the latter of which is slightly red-shifted, indicative of the formation of closer π–π stacks. The film absorption edge of **P75** and PBDB-T are around 875 and 690 nm, corresponding to E_gs of 1.42 and 1.80 eV, respectively. The electrochemical cyclic voltammetry (CV) spectra are displayed in Figure S2b, showing a distinct reversible oxidation potential, suggestive of p-type semiconducting characteristics, which determines the HOMO energy levels. Accordingly, the LUMO energy levels are estimated by the difference of E_g and HOMO level. Table S2 summarizes the detailed absorption and electrochemical parameters of them. The LUMO level of **P75** is downshifted by ~0.4 eV relative to PBDB–T, and thus the LUMO level offsets between **P75** and Y6 acceptor are notably narrowed (**Figure 1**b), which aids in reducing energy loss in NF-OSCs without affecting efficient charge separation. Besides, **P75** shows such a HOMO energy level that is downshifted than PBDB–T yet upshifted than PM6, which could permit a V_{OC} between those of two devices. Deeper HOMO and LUMO energy levels of **P75** than PBDB–T are attributed to a stronger electronegativity of DPP unit than BDD moiety. It can be concluded that halogen-free polymer donor (e.g., **P75**) by a slight addition of highly electron-deficient (e.g., DPP) unit better matches the state-of-the-art NFAs (e.g., Y6) than PBDB–T yet performs inferior to PM6. This is further supported by their NF-OSCs fabricated in the absence of any additives or annealing treatment, whose photocurrent density–voltage (*J*–*V*) curves and external quantum efficiency (EQE) spectra are displayed in Figure S3 along with the detailed device parameters listed in Table S3. The **P75**:Y6 blend device yields a higher PCE of 10.28% than the PBDB–T based device showing a PCE of 9.24% along with J_{SC} of 19.2 mA cm^{-2}, V_{OC} of 0.78 V and fill factor (FF) of 65%. The enhancement mainly benefits from a simultaneous increase of J_{SC} (22.6 mA cm^{-2}) and V_{OC} (0.81 eV) due to an incorporation of 25 mol% highly electron-

deficient DPP unit in the main chain in **P75**. When compared to the paradigm PM6:Y6 blend device—mostly treated with 0.5% chloronaphthalene (CN) additive and thermal annealing at 110 °C for 10 min—which resulted in a best PCE of 15.7% along with J_{SC} = 25.3 mA cm^{-2}, V_{OC} = 0.83 eV and FF = 74.8%,[9] however, the above V_{OC} is notably lower owing to the higher HOMO energy level of **P75** (−5.43 eV) than PM6 (−5.56 eV), whereas both inferior J_{SC} and FF can be ascribed to the more compact and ordered π-stacks in PM6-based blend (3.61 Å) than that of **P75** (3.64 Å as seen below). The stronger intermolecular interaction of PM6-based blend arises presumably from additional additive/annealing treatments, while the favorable film morphology of **P75**-based blend is independent of treatments as seen from the following studies.

Our previous work has established that a fullerene derivative acceptor would largely enhance electron extraction and reduce charge recombination.[48,49] Inspired by it, we next employed $PC_{71}BM$ as a third component in the **P75**:Y6 binary blend with a **P75**:Y6:$PC_{71}BM$ ratio of 1.5:1.4:0.1, 1.5:1.3:0.2 and 1.5:1.2:0.3 wt% in ternary blends, which are denoted as $\mathbf{T}_{0.1}$, $\mathbf{T}_{0.2}$ and $\mathbf{T}_{0.3}$ with respect to $PC_{71}BM$ wt%, respectively, for simplicity in the following discussion. The optical absorption of binary and ternary blend films in comparison to their neat films are shown in **Figure 1**c. The increased absorption intensity in the short wavelength of 350−450 nm afforded by $PC_{71}BM$ is conductive to the J_{SC} enhancement to some extent. In addition, slight blue-shifts in the absorption of the ternary blend film are observed, suggesting $PC_{71}BM$ would affect the molecular aggregation during solvent evaporation in spin-coating of the blend film.

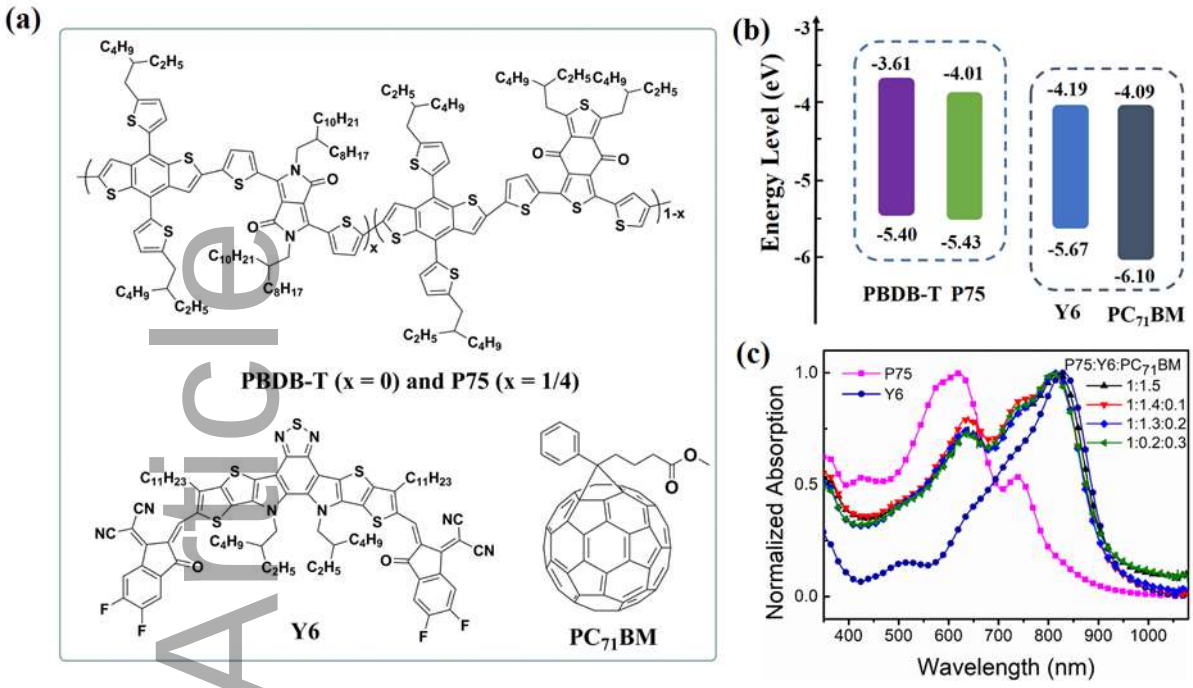

Figure 1. (a) Molecular structures, (b) energy level diagram, and (c) optical absorption spectra of **P75** and PBDB–T donors as well as Y6 and $PC_{71}BM$ acceptors.

To clarify such a microstructural dependence on $PC_{71}BM$, grazing-incidence wide-angle X-ray scattering (GIWAXS) technique was then used to probe the molecular packing and orientation of the blend films. As shown in **Figure 2**, it is clearly seen that all the blend films show preferential face-on molecular orientation. The **P75**:Y6 blend exhibits a notable (010) peak at ~1.725 $Å^{-1}$, characteristic of π-π stacks in the out-of-plane (OOP) direction with a distance of 3.641 Å and a crystallinity coherent length (CCL) of 13.78 Å (**Figure 2**a,e). The lamellar peak located at ~0.285 $Å^{-1}$ corresponds to a *d*-spacing of 22.035 Å along the in-plane (IP) direction. When adding $PC_{71}BM$ from 0.1, 0.2 to 0.3 wt%, the ternary blend films—$\mathbf{T}_{0.1}$, $\mathbf{T}_{0.2}$ and $\mathbf{T}_{0.3}$ (**Figure 2**b–d,e)—display π-stack spacings / CCLs of 3.636 / 14.65, 3.638 / 14.12 and 3.645 / 11.68 Å in OOP direction at 1.727, 1.726 and 1.723 $Å^{-1}$, respectively, coupled with the lamellar peaks varying from 0.296 to 0.316 $Å^{-1}$ in IP direction. The smaller $PC_{71}BM$ wt% yet the bigger CCL in the ternary blend, the higher crystallinity of blend film, indicative of larger-scale phase-segregation. Furthermore, transmission electron microscopy (TEM) and atomic force microscopy (AFM) were utilized to directly image the

internal and surficial morphologies of these blend films. As shown in **Figure 2**f, homogeneous morphologies are observed in all four blend films, indicative of excellent miscibility. From **Figure 2**g, the root-mean-square (RMS) surface roughness of binary blend film is 3.2 nm while those of $\mathbf{T}_{0.1}$, $\mathbf{T}_{0.2}$ and $\mathbf{T}_{0.3}$ ternary blend films are 3.7, 6.0, and 9.4 nm, respectively. Besides, well-distributed interpenetrated nano-fibrillar structures are found on the surface of all the blend films. Compared to the binary blend film, however, the nanoscale phase-separation gradually becomes increasingly noticeable with an increasing $PC_{71}BM$ ratio in ternary blends from AFM, which is consistent with the increased RMS. In short, by combining the above-discussed X-ray scattering and microscopical results, a favorite microstructure of the blend film is correlated with a ratio of **P75**:Y6:$PC_{71}BM$ = 1:1.4:0.1 wt%, that is, $\mathbf{T}_{0.1}$.

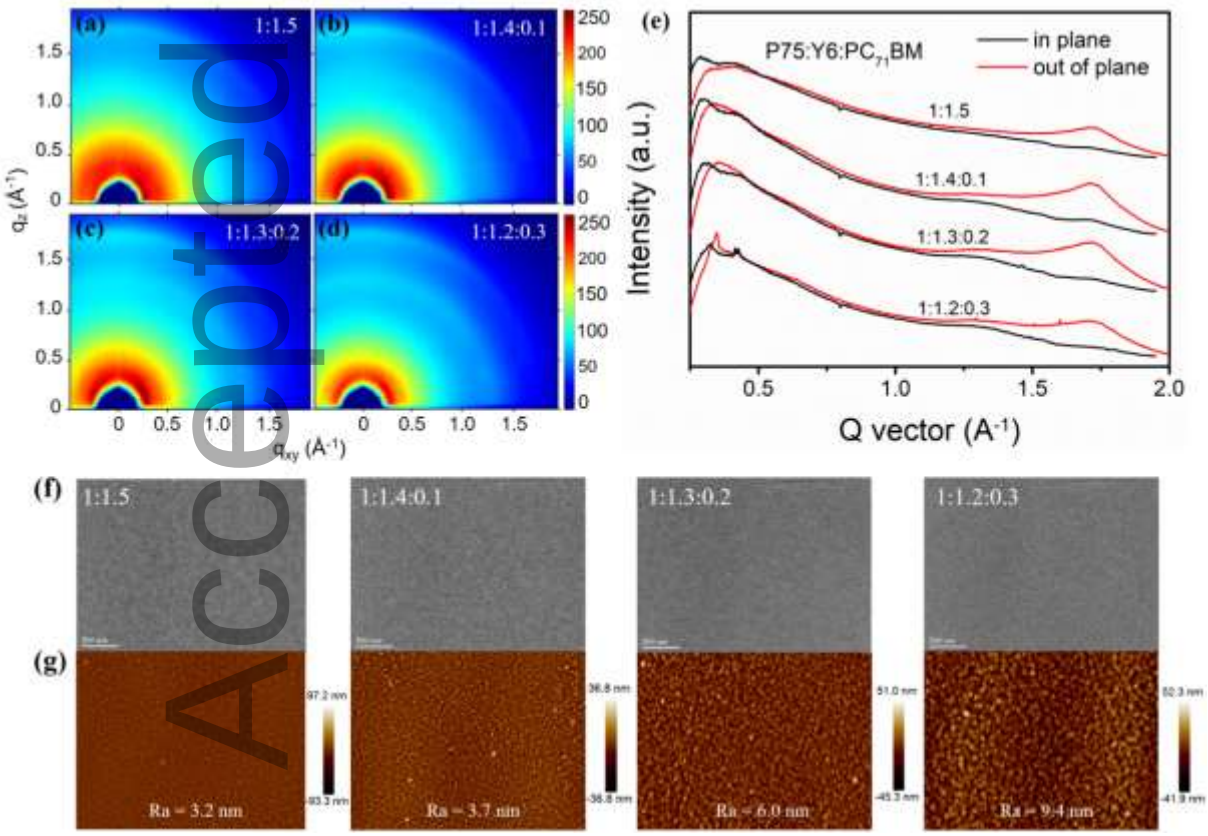

Figure 2. (a–d) GIWAXS profiles and (e) their corresponding IP and OOP line-cuts, (f) HR-TEM and (g) tapping-AFM height images of the **P75**:Y6:$PC_{71}BM$ blend films with various component ratios.

As such, we further investigated the impact of $PC_{71}BM$ ratio on the performance of additive/annealing-free ternary NF-OSCs. The *J–V* curves and EQE spectra of **ternary** blend devices in comparison to binary **P75**:Y6 reference are shown in **Figure 3**. **Table 1** lists the detailed photovoltaic parameters and the integrated photocurrent of the device as calculated from the EQE spectra within the margin of error (5%), which agrees well with the J_{SC} values acquired from the *J–V* curves. By starting to add 0.1 wt% $PC_{71}BM$, the $\mathbf{T}_{0.1}$ device affords an impressive PCE of 12.20%, which arises primely from a remarkable improvement of J_{SC} and FF up to 25.0 mA cm^{-2} and 61%, respectively, without affecting V_{OC}. As the $PC_{71}BM$ content is further increased to 0.2 ($\mathbf{T}_{0.2}$) and 0.3 wt% ($\mathbf{T}_{0.3}$), however, the devices become slightly and even worse, in the latter of which V_{OC}, J_{SC} and FF coincidently drop to 0.80 V, 21.9 mA cm^{-2} and 57%, giving rise to an inferior efficiency of ~10%. Clearly, these results suggest that a slight incorporation of $PC_{71}BM$ offers additional electron-transporting paths to facilitate charge transport and collection, thus increasing both J_{SC} and FF, accompanied by little energy loss (that is, nearly unchanged V_{OC});[50,51] yet an excessive addition could cause an increasingly rougher blend film, i.e., severe phase-separation, as evidenced by Figure 2, which is unfavorable for exciton dissociation and charge transport. As a result, 0.1 wt% $PC_{71}BM$ addition (i.e., $\mathbf{T}_{0.1}$ blend) yields an optimal film morphology, which is the most beneficial for device enhancement.

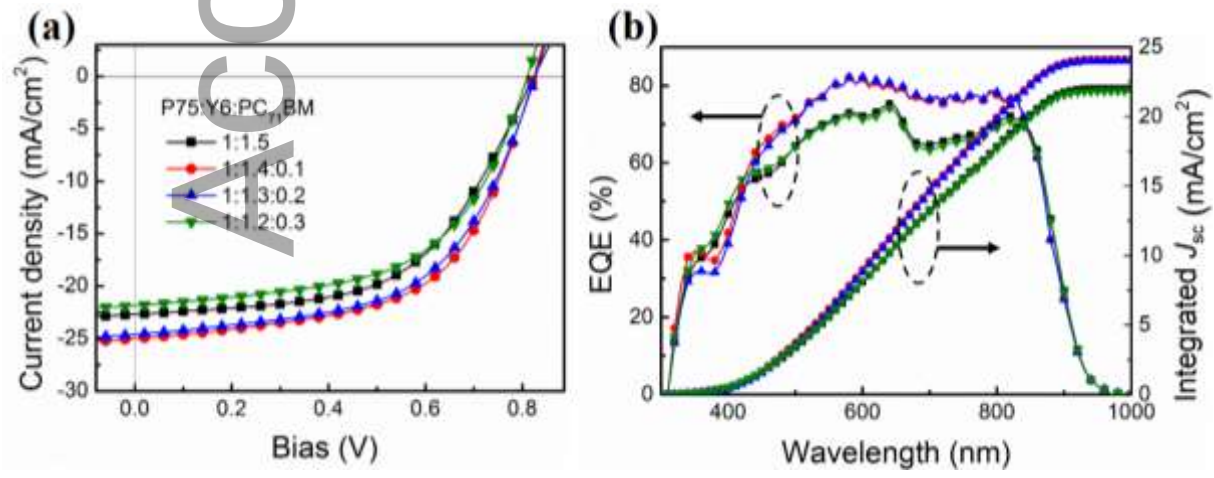

Figure 3. (a) *J–V* curves and (b) EQE spectra of the **P75**:Y6:$PC_{71}BM$ blend at different composition ratios.

Table 1. A summary of photovoltaic parameters of ternary **P75**:Y6:$PC_{71}BM$ based OSCs at a variety of weight ratios

P75:Y6:$PC_{71}BM$	V_{OC} (V)	J_{SC} (mA cm^{-2})	J_{SC} [a] (mA cm^{-2})	**FF** (%)	**PCE** (%)
1:1.5	0.81	22.6	22.0	58	10.28
1:1.4:0.1	0.81	25.0	24.1	61	12.20
1:1.3:0.2	0.82	24.5	24.0	60	11.43
1:1.2:0.3	0.80	21.9	21.8	57	9.99

[a] J_{SC} values are calculated from the EQE curves

In order to understand the photophysical property of as-fabricated OSCs devices, the photocurrent (J_{ph}) as a function of the effective voltage (V_{eff}) is plotted in **Figure 4**a. The probability of the exciton dissociation is expressed by $\eta_{diss} = J_{ph} / J_{sat}$ where $J_{ph} = J_L - J_D$ is the current density under illumination, V_{eff} is the bias voltage when $J_{ph} = 0$ and J_D is the current density under dark, J_{sat} is the current density when J_{ph} saturates at $V_{eff} \geqq 2$ V. Also, the charge collection efficiency is calculated by $\eta_{coll} = J_{power} / J_{sat}$, where J_{power} is the current density at the maximum power point.[52] As manifested in **Table 2**, the J_{sat} and η_{diss}/η_{coll} values of **P75**:Y6-based binary device are 27.09 mA cm^{-2} and 83%/68%, respectively. The J_{sat} values of $\mathbf{T}_{0.1}$, $\mathbf{T}_{0.2}$ and $\mathbf{T}_{0.3}$ blend devices are 27.40, 27.03 and 26.99 mA cm^{-2}, respectively, corresponding to the η_{diss}/η_{coll} values of 83%/68%, 90%/73%, 88%/72% and 81%/64%. Obviously, the $\mathbf{T}_{0.1}$ device gives comparatively higher values of J_{sat} and η_{diss}/η_{coll}, which account for the best EQE and J_{SC}. Meanwhile, the equation of $G_{MAX} = J_{ph}/qL$ was used to estimate the maximum exciton generation rate (G_{MAX}) under the J_{sat} of the devices, where q and L represent the electron charge and the thickness of the active layer, respectively. As can be seen from **Table 2**, the G_{MAX} values of $\mathbf{T}_{0.1}$, $\mathbf{T}_{0.2}$ and $\mathbf{T}_{0.3}$ ternary devices are determined to be 1.71, 1.70 and 1.68×10^{24} cm^{-3} s^{-1}, respectively, which is consistent with the corresponding J_{SC} because G_{MAX} is closely related to the light absorption of the active layer.

Time-resolved photoluminescence (TRPL) spectroscopy was employed to further elaborate on the role of the third-component $PC_{71}BM$ on charge extraction as depicted in Figure S4 and Table S4. The emission lifetime (τ) of **P75**:Y6 based binary device is 1.90 ns, whereas it significantly decays to 0.69, 0.89, and 1.84 ns for $\mathbf{T}_{0.1}$, $\mathbf{T}_{0.2}$ and $\mathbf{T}_{0.3}$ ternary blend devices, respectively, suggesting that the exciton dissociation and extraction are promoted as a result of additional electron-transporting paths afforded by $PC_{71}BM$.[53,54] Remarkably, $\mathbf{T}_{0.1}$ exhibits the even faster PL quenching with a minimum τ, indicating the best charge dissociation and collection efficiency. In addition, the space charge limited current (SCLC) method was used to assess the charge transport characteristics of blend films including hole (μ_h) and electron (μ_e) mobilities as shown in **Figure 4**b and c. As seen in Table S4, the μ_h/μ_e of optimal $\mathbf{T}_{0.1}$ attains a most balanced transport value of 0.46, which is responsible for superior FF.[51]

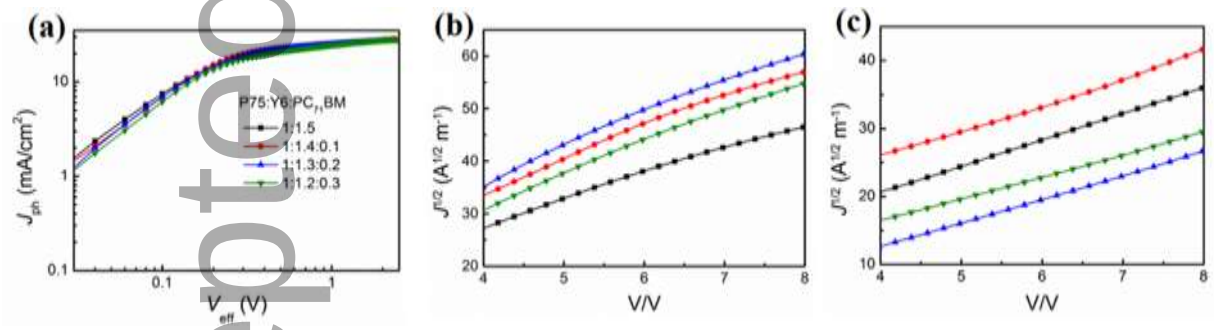

Figure 4. (a) J_{ph}–V_{eff} curves (b) electron- and (c) hole-only devices based on the **P75**:Y6:$PC_{71}BM$ blend at different weight ratios.

Table 2. Exciton dissociation and collection efficiency of OSCs based on **P75**:Y6:$PC_{71}BM$ at different compositional ratios

P75:Y6:$PC_{71}BM$	J_{sat} (mA cm^{-2})	η_{diss} (%)	η_{coll} (%)	G_{MAX} (cm^{-3} s^{-1})
1:1.5	27.09	83	68	1.69×10^{24}
1:1.4:0.1	27.40	90	73	1.71×10^{24}
1:1.3:0.2	27.03	88	72	1.70×10^{24}
1:1.2:0.3	26.99	81	64	1.68×10^{24}

Furthermore, the dependence of J_{SC} on light intensity was examined to unveil the non-geminate recombination dynamics as shown in **Figure 5**a. The exponential factor S value of the power law equation $J_{SC} \propto P_{light}^{S}$ represents the degree of bimolecular recombination.[55] As compared to **P75**:Y6 binary device (S = 0.92), the S values of $\mathbf{T}_{0.1}$, $\mathbf{T}_{0.2}$ and $\mathbf{T}_{0.3}$ ternary devices are estimated to be 0.95, 0.93 and 0.91, respectively, in which $\mathbf{T}_{0.1}$ shows the most effectively suppressed biomolecular recombination with S value comparatively closer to 1 than others. A relation of $V_{OC} \propto \ln(P_{light}) \times kT/q$ was used to identify the dominant charge recombination mechanism where k is the Boltzmann constant, T is the temperature and q is the electron charge. The slope of kT/q is considered to be a bimolecular dominant recombination, which however would deviate due to the trap-assisted recombination.[56] As shown in the **Figure 5**b, the plotted slopes of binary and ternary devices are determined to be 1.47, 1.24, 1.40, and 1.52 kT/q, respectively, among which the optimal $\mathbf{T}_{0.1}$ device yields the lowest slope, implying the existence of the least trap-assisted carrier recombination in NF-OSCs.

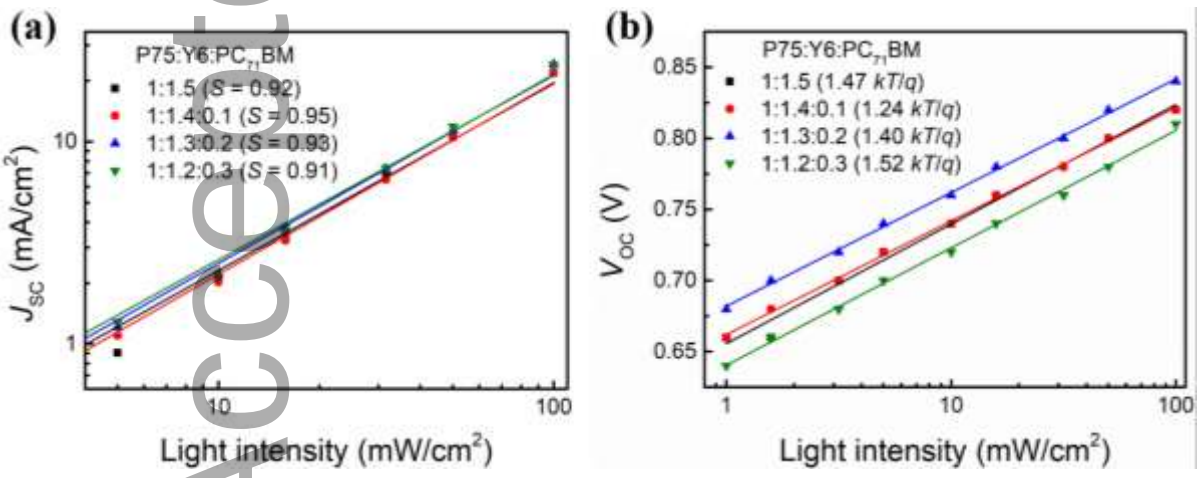

Figure 5. Dependences of light-intensity on both (a) J_{SC} and (b) V_{OC} of devices based on the **P75**:Y6:$PC_{71}BM$ blends at different weight ratios.

To further understand the influence of $PC_{71}BM$ addition on the charge carrier dynamics, we investigated the excited state dynamics of blend films by transient absorption (TA) spectroscopy. **Figure 6** shows the TA spectra of binary and ternary blend films excited at both 800 and 400 nm with

corresponding singular value decomposition (SVD) analysis as discussed below. Upon photo-excitation at 800 nm, the TA spectrum of neat Y6 film reflects a fast hot exciton cooling (2 ps) and a slow 1S exciton recombination (208 ps) (**Figure 6**a). In binary (**Figure 6**b) and ternary blend samples (**Figure 6**c–e), fast sub-picosecond hole transfer from Y6 to the HOMO level of the donor can be derived. The interfacial recombination between the injected holes at the HOMO level of **P75** and the remaining electrons at the LUMO level of Y6 occurs within 141–217 ps (Please refer to SI for the detailed TA analysis). Such a process is fast and independent of the $PC_{71}BM$ addition, meaning the hole dynamics cannot be modulated by the intercalation of the fullerene component at the open-circuit (OC) condition.

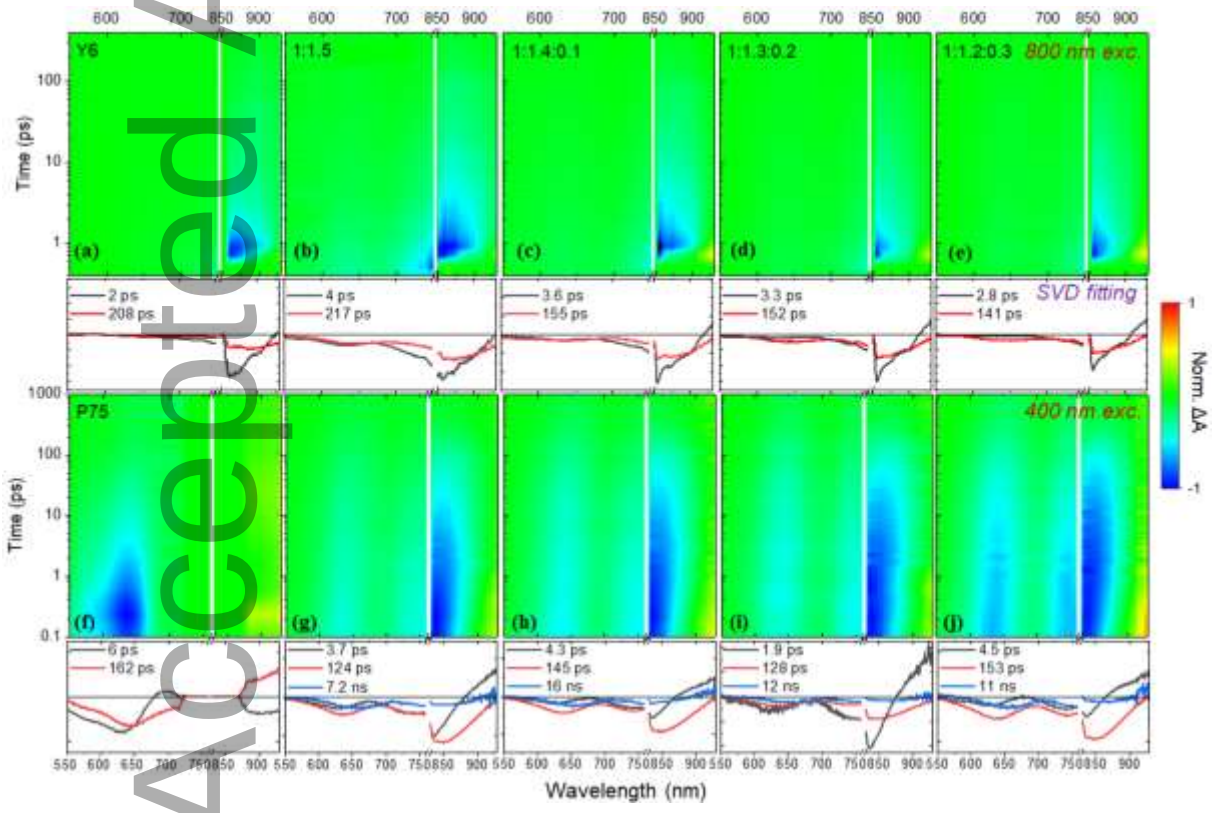

Figure 6. TA spectra of the **P75**:Y6:$PC_{71}BM$ blend films with various weight ratios in comparison to neat Y6 and **P75** films with (a–e) 800 nm and (f–j) 400 nm photo-excitation.

Subsequently, upon 400 nm high-energy photon excitation, both **P75** and Y6 are excited. The TA spectra of neat **P75** (**Figure** 6f), binary (**Figure 6**g) and ternary blend samples (**Figure 6**h–j) exhibit very similar dynamics to those photo-excited in 800 nm as shown above. However, we can

extract one additional nanosecond component in binary and ternary samples, which is attributed to the free carriers in **P75** (blue curves in the SVD fitting) (also refer to SI for detailed TA analysis). The lifetimes of these components are increased with the $PC_{71}BM$ addition up to 16 ns at an optimal weight ratio of 1:1.4:0.1 and subsequently decreased. This increasing and then decreasing trend is consistent with the TRPL results. We argue the longest free carrier lifetime indicate the least carrier recombination during charge transport through the active layer, which is dominantly responsible for the high J_{SC} of $\mathbf{T}_{0.1}$ device.

These above results indicate that the excitons photo-generated in Y6 based binary or ternary blend films would quickly recombine within 150 ps even if the hole is transferred to **P75** within picosecond, a fingerprint of the charge-transfer state (CTS) formation. We have previously revealed such CTS in mixed ITIC and IEICO-4F acceptors based blend films.[46] In the present **P75**:Y6:$PC_{71}BM$ blend, CTS is only formed when holes are transferred from Y6 to **P75**. This can be due to the more efficient vibrational relaxation of holes in **P75** compared with electrons in Y6 which dominates the charge trapping by CTS. Therefore, the CTS-mediated hole transfer should be the bottleneck that affects the charge separation at the interface of **P75**:Y6. We just confirmed above that the charge recombination at the CTS is independent of the $PC_{71}BM$ addition in OC condition. However, during the functioning of the solar cell devices, the applied external bias will tune the interfacial band bending that presumably influence the CTS formation and dissociation. In order to justify this, we conducted TA on the working device of **P75**:Y6:$PC_{71}BM$ blend with an applied external bias mimicking the functioning mode in solar cells, as illustrated in **Figure 7**a. **Figure 7**b shows the TA kinetics at **B2** of **P75** at open-circuit and a forward bias of 0.5 V with 800 nm excitation for all the binary and ternary blend devices. Compared to TA kinetics at OC, the TA kinetics at 0.5 V bias of binary and ternary $\mathbf{T}_{0.1}$ devices decay faster at the first several ps and then become much slower at the long-time delay. Since the forward bias posed on the devices flattens the difference of HOMO/LUMO energy levels between donor and acceptor, the energy level of singlet CTS (^{1}**CT**)

should also be levitated, as shown in **Figure 7**c. Consequently, it would hinder the CTS trapping and facilitate the charge separation directly to the free charge (FC) state (denoted as process **1**). This explains the accelerated GB recovery at the early timescale of the TA kinetics as shown in **Figure 7**b. The separated free charges can be backward-recombined to **^{1}CT** after random diffusion yet after a long time (denoted as process **2**). We notice such phenomenon is pronounced in $\mathbf{T}_{0.1}$ but absent in other ternary blend films with more $PC_{71}BM$ addition where the TA kinetics at OC and 0.5 V bias are entirely identical (**Figure 7**b). This indicates the original CTS in $\mathbf{T}_{0.1}$ is the shallowest, enabling the exciton dissociation by 0.5 V bias. The CTS energy E_{CT} is contributed by the energetic difference between the donor's HOMO and the acceptor's LUMO levels and the interface Columbic energy (ΔE_c). In a typical D-A system, the CT emission energy is proportional to the inverse local static dielectric constant, i.e., $\Delta em \propto 1/\varepsilon$.[56] Therefore, we believe the $PC_{71}BM$ addition mainly modulates the CT energy by weakening the local dielectric screening and increase Δ. However, such an effect should only be valid when $PC_{71}BM$ is intercalated homogenously between donor and acceptor in our case, while over-addition of $PC_{71}BM$ in the blend may induce severe phase segregation that declines the screening effect. The shallowest CTS in optimal $\mathbf{T}_{0.1}$ leads to the smallest CT binding energy, which guarantees the highest CT dissociation efficiency according to the Onsager−Braun model.[41] This is of a typical advantage to enhance FF due to the reduced carrier recombination arising from the CTS directly to the ground state.[58]

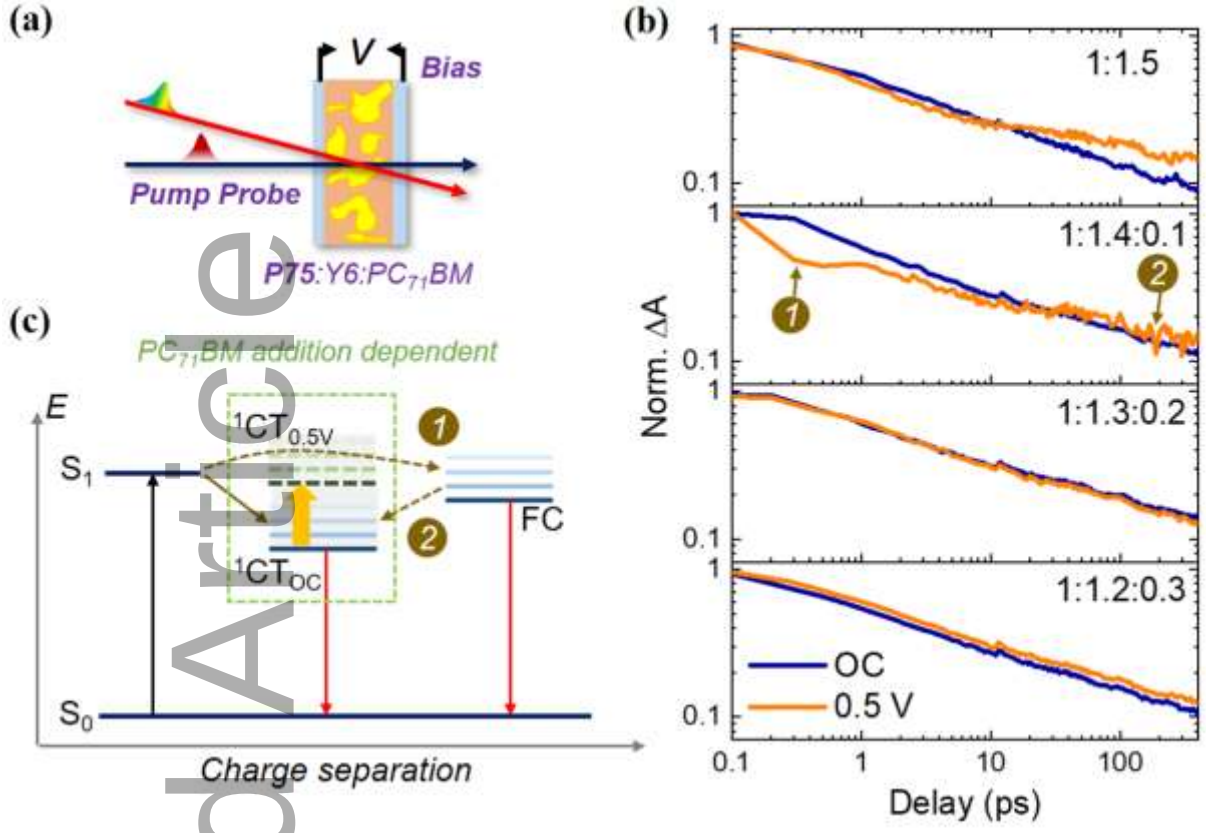

Figure 7. In-situ TA measurement: (a) Schematic setup, (b) measured spectra on ternary **P75**:Y6:$PC_{71}BM$ device at open-circuit and forward-bias conditions when pumped at 800 nm and (c) the proposed photophysics with regard to modified CTS by applying a bias in the blend films.

3. Conclusions

In conclusion, we have successfully incorporated electron-deficient DPP moiety into the paradigm π-backbone of PBDB-T donor and developed halogen-free copolymer donors as best exemplified by **P75**. Compared to the reference PBDB–T, **P75** ensures a narrower E_g of ~1.42 eV, deeper LUMO/HOMO energy levels of –4.01/5.43 eV and extended optical absorption owing to stronger electronegativity of DPP unit. Both notably high V_{OC} (0.81 eV) and J_{SC} (22.60 mA cm^{-2}) are obtained for the **P75**:Y6 blend device, yielding an encouraging PCE of 10.28%. Interesting, a slight addition of $PC_{71}BM$ into the binary system with an optimal ratio of 1:1.4:0.1 boosted the best PCE to 12.20% accompanied by significantly improved J_{SC} of 25.0 mA cm^{-2} yet unaffected V_{OC} of 0.81 eV. Time-resolved spectroscopical studies on both neat and blend films indicate the extremely efficient photo-

induced interfacial charge transfer between **P75** and Y6 while $PC_{71}BM$ addition further ensures the prolonged free carrier lifetime after photo-charge separation thanks to its efficient electron extraction. More importantly, the TA measurement on the device configuration with applied bias suggests the $PC_{71}BM$ addition can modify the CTS and CT energy by weakening the local dielectric screening. Note that in the optimal device with 0.1 wt% $PC_{71}BM$ addition, the CT binding energy is the smallest, which guarantees the best-efficient CT dissociation and thus rationalizes the highest J_{SC} and FF. In short, the developed halogen-free polymer donors exemplify cost-effective synthetic routes for tailorable molecular structures and blend films to match NFAs and achieve highly efficient nonfullerene solar cells.

4. Experimental Section

Materials: Chemicals and reagents were purchased from commercial sources and used without further purification unless otherwise indicated. All the solvents were dried by the activated molecular sieve and all the reactions were performed under a nitrogen atmosphere.

Synthesis of **P75**: A mixture of monomer DPP (50.96 mg, 0. 05 mmol), BDD (115.01 mg, 0.15 mmol), BDT (180.91 mg, 0.20 mmol), $Pd_2(dba)_3$ (3.66 mg, 0.004 mmol), P(o-Tolyl)$_3$ (4.87 mg, 0.016 mmol) were added into Schlenk tube. A 6 mL of anhydrous chlorobenzene was added to the mixture. The whole system was stirred at 100 °C for 18 hours under N_2 atmosphere. The reaction was terminated when the mixed solution in tube had been a gel. After polymerization, the mixture was cooled down to room temperature and added some methanol to gain the precipitate of polymer. The polymer was purified sequentially using Soxhlet extractions with methanol, petroleum ether, Acetone, dichloromethane, chloroform for 24 hours each, and dried to gain dark solid polymer (125 mg, yield: 50%).[59] GPC: M_n = 35.11 kDa, M_w = 50.30 kDa, PDI = 1.46; Anal. Calcd. for Chemical Formula: C292H360N2O8S30, C, 70.14; H, 7.19; N, 0.49; S, 19.59. Found: C, 69.21; H, 7.10; N, 0.67; S, 18.74.

Synthesis of PBDB–T: PBDB–T was gained following the same procedure as that of the polymer of P75 except content level. The monomer BDD (153.30 mg, 0.15 mmol), BDT (180.91 mg, 0.20 mmol), $Pd_2(dba)_3$ (3.66 mg, 0.004 mmol), P(o-Tolyl)$_3$ (4.87 mg, 0.016 mmol) were added (the reaction was stopped for 24 hours when the mixed solution in tube had been a gel) and the dark solid polymer was gained (190 mg, yield: 80%).[59] GPC: M_n = 26.93 kDa, M_w = 40.75 kDa, PDI = 1.51; Anal. Calcd for Chemical Formula: C68H78O2S8, C, 68.99; H, 6.64; S, 21.66. Found: C, 65.02; H, 7.90; S, 18.79.

Polymer Characterization: The thermogravimetric analyses (TGA) were conducted at heating rate of 100 °C min^{-1} under nitrogen gas flow and were taken on a Simultaneous Thermal Analyzer (TSA) instrument (STA449C/449F5). High temperature gel permeation chromatography (HT-GPC) was carried out on a ShimadzuSIL-20A liquid chromatography instrument using 1,2,4-trichlorobenzene (TCB) as eluent at 150 °C with polystyrenes as standards. UV-vis spectra were performed on a PerkinElmer Lambda 20 UV-vis spectrophotometer. Element Analyzer (EA) were measured Vario EL cube. Cyclic voltammetry (CV) measurements were record with a three-electrode cell under a nitrogen atmosphere in a deoxygenated anhydrous acetonitrile solution of tetra-n-butylammonium hexafluorophosphate (0.1 M). A platinum disk electrode, platinum wire, and Ag/AgCl electrode were used as a working electrode, a counter electrode, and a reference electrode separately, and the film of polymers were coated on the surface of platinum disk electrode for evaluation. The CV curves were calibrated using ferrocene/ferrocenium (Fc/Fc^+) redox couple as an external standard, which was performed at the same conditions as other samples.

Thin Film Characterization: High-resolution transmission electron microscopy (TEM) imaging was performed on Tecnai G2 F20 S-Twin microscope at an accelerating voltage of 200 kV. Bruker Dimension Edge atomic force microscope (AFM) in the tapping mode was utilized to image blend film topographies. The height images were gained at a scan rate of 1 Hz with a resolution of 256 × 256 pixels using a silicon etched tip, which has a resonance frequency of ~300 kHz and a spring

constant of ~40 N m^{-1}. GIWAXS patterns were acquired by beamline BL14B1 at Shanghai Synchrotron Radiation Facility (SSRF). Transient absorption experiments were performed by using a femtosecond pump-probe setup in nitrogen atmosphere. Laser pulses (800 nm, 80 fs pulse length, 1 kHz repetition rate) were generated by a regenerative amplifier (Spitfire XP Pro) seeded by a femtosecond oscillator (Mai Tai SP, both Spectra Physics). The pump pulses at 400 nm and 800 nm were generated by an optical parametric amplifier (Topas, Light Conversion). The used excitation photon fluxes are 1×10^{12} photons/cm^2/pulse. For the probe, we used the super-continuum S3 generation from a thin CaF_2 plate. The mutual polarization between pump and probe beams was set to the magic angle (54.7°) by placing a Berek compensator in the pump beam. The probe pulse and the reference pulse were dispersed in a spectrograph and detected by a diode array (Pascher Instruments). In order to avoid photo-damage, the sample was moved to a fresh spot after each time delay point. Global SVD analysis was performed with the Glotaran software package (http://glotaran.org). These methods yield more accurate fits of rate constants because they treat the full data set as a whole. A simple sequential decay model with various components is chosen for every fitting.

Device Fabrication and Measurements: Solar cell devices were fabricated with a conventional device structure of ITO/PEDOT:PSS/active layer/PFN-Br/Ag. The ITO-coated glass substrates were sonicated successively with detergent, deionized water, acetone and isopropanol, and dried with nitrogen flow. Immediately prior to device fabrication, the substrates were cleaned by oxygen plasma for 20 min. A layer of PEDOT:PSS was then spin-coated onto the ITO and annealing at 130 °C for 20 min. The active layer was stirred at room temperature for overnight and was obtained by spinning from chloroform (CF) solution as the processing additive at 3000 r.p.m. for 50 s. The constant weight ratio of donor/acceptor is 1:1.5 with a total concentration of 15 mg mL^{-1}. And then, PFN-Br solution (in CH_3OH) was spin-coated as electron transfer layer. Finally, Ag (100 nm) was evaporated at a vacuum of ~2.5×10^{-4} Pa to form the top electrode. The *J–V* data were acquired from a Keithley 2400

source–meter unit. The light *J–V* curves were measured under light illumination with a Newport-Oriel (Sol3A Class AAA Solar Simulator, 94043A) AM 1.5G light source operating at an intensity of 100 mW cm^{-2}. The light intensity was calibrated by a certified Oriel reference cell (91150V) and verified with a NREL calibrated, filtered silicon diode (Hamamatsu, S1787-04). External quantum efficiency (EQE) spectra were measured on a commercial EQE set-up (QE-R, Enli Technology Co., Ltd). A calibrated silicon diode with a known spectral response was used as a reference. Hole and electron mobilities were attained by using the space charge limited current (SCLC) method.[60] The structure of ITO/PEDOT:PSS/active layer/MoO_3 /Ag was used for hole-only devices and the structure of ITO/ZnO/active layer/PFN-Br/Ag was used for electron-only devices, respectively. The SCLC mobilities were calculated by MOTT–Gurney equation:

$$J = \frac{9\varepsilon_0\varepsilon_r\mu V^2}{8L^3}$$

where J is the current density, ε_0 is the dielectric constant of empty space, ε_r is the relative dielectric constant of active layer materials which is taken to be 3 in the calculation, μ is the charge mobility, V is the internal voltage in the device, and L the thickness of the active layers. V can be calculated as $V = V_{appl} - V_{bi}$, where V_{appl} is the voltage applied to the devices, V_{bi} is the built-in voltage from the relative work function difference between the two electrodes.

Supporting Information

Supporting Information is available from the Wiley Online Library or from the author.

Conflicts of interest

There are no conflicts to declare.

Acknowledgements

We acknowledged the support of International Cooperation Project of Ministry of Science and Technology (MOST) under grant No. 2017YFE0107800 (Z.L.), Science and Technology Commission of Shanghai Municipality (STCSM) under grant No. 20XD1400500 (Z.L.), National Natural Science Foundation of China (NSFC)–The Swedish Foundation for International Cooperation in Research and Higher Education (STINT) under grant No. 5191101797 (Z.L.) and

Danish Council for Independent Research No. 7026-0037B and Swedish Research Council No. 2017–05337 (K.Z.). The authors also gratefully thank for the beam time and technical supports provided by the BL14B1 GIWAXS beamline at Shanghai Synchrotron Radiation facility (SSRF).

Received: ((will be filled in by the editorial staff))
Revised: ((will be filled in by the editorial staff))
Published online: ((will be filled in by the editorial staff))

[1] R. Ma, Y. Tao, Y. Chen, T. Liu, Z. Luo, Y. Guo, Y. Xiao, J. Fang, G. Zhang, X. Li, X. Guo, Y. Yi, M. Zhang, X. Lu, Y. Li, H. Yan, *Sci. China Chem.* **2021**, *64*.

[2] X. Xu, K. Feng, Z. Bi, W. Ma, G. Zhang, Q. Peng, *Adv. Mater.* **2019**, *31*,1901872.

[3] R. Ma, G. Li, D. Li, T. Liu, Z. Luo, G. Zhang, M. Zhang, Z. Wang, S. Luo, T. Yang, F. Liu, H. Yan, B. Tang, *Sol. RRL* **2020**, *4*, 2000250.

[4] Q. Yue, H. Wu, Z. Zhou, M. Zhang, F. Liu, X. Zhu, *Adv. Mater.* **2019**, *31*,1904283.

[5] S. Li, L. Zhan, Y. Jin, G. Zhou, T. K. Lau, R. Qin, M. Shi, C. Z. Li, H. Zhu, X. Lu, F. Zhang, H. Chen, *Adv. Mater.* **2020**, *32*, 2001160.

[6] J. Ge, L. Xie, R. Peng, B. Fanady, J. Huang, W. Song, T. Yan, W. Zhang, Z. Ge, *Angew. Chem. Int. Ed.* **2020**, *59*, 2808.

[7] X. Liu, C. Zhang, C. Duan, M. Li, Z. Hu, J. Wang, F. Liu, N. Li, C. J. Brabec, R. A. J. Janssen, G. C. Bazan, F. Huang, Y. Cao, *J. Am. Chem. Soc.* **2018**, *140*, 8934.

[8] Y. Zhang, C. Duan, L. Ding, *Ding, Sci. Bull.* **2020**, *65*, 2040.

[9] G. Chai, Y. Chang, Z. Peng, Y. Jia, X. Zou, D. Yu, H. Yu, Y. Chen, P. C. Y. Chow, K. S. Wong, J. Zhang, H. Ade, L. Yang, C. Zhan, *Nano Energy* **2020**, *76*, 105087.

[10] T. Liu, R. Ma, Z. Luo, Y. Guo, G. Zhang, Y. Xiao, T. Yang, Y. Chen, G. Li, Y. Yi, X. Lu, H. Yan, B. Tang, *Energy Environ. Sci*. **2020**,*13*, 2115.

[11] R. Zhou, Z. Jiang, C. Yang, J. Yu, J. Feng, M. A. Adil, D. Deng, W. Zou, J. Zhang, K. Lu, W. Ma, F. Gao, Z. Wei, *Nat. Commun.* **2019**, *10*, 5393.

[12] K. Weng, L. Ye, L. Zhu, J. Xu, J. Zhou, X. Feng, G. Lu, S. Tan, F. Liu, Y. Sun, *Nat. Commun.* **2020**, *11*, 2855.

[13] C. Duan, K. Gao, J. J. Franeker, F. Liu, M. M. Wienk, R. A. J. Janssen, *J. Am. Chem. Soc.* **2016**, *138*, 10782.

[14] S. Dong, T. Jia, K. Zhang, J. Jing, F. Huang, *Joule* **2020**, *4*, 2004.

[15] J. Yuan, Y. Zhang, L. Zhou, G. Zhang, H.-L. Yip, T.-K. Lau, X. Lu, C. Zhu, H. Peng, P. A. Johnson, M. Leclerc, Y. Cao, J. Ulanski, Y. Li, Y. Zou, *Joule* **2019**, *3*, 1140.

[16] R. Ma, T. Liu, Z. Luo, K. Gao, K. Chen, G. Zhang, W. Gao, Y. Xiao, T. Lau, Q. Fan, Y. Chen, L.

Ma, H. Sun, G. Cai, T. Yang, X. Lu, E. Wang, C. Yang, A. K. Jen, H. Yan, *ACS Energy Lett.* **2020**, *5*, 2711.

[17] Y. Cui, H. Yao, J. Zhang, K. Xian, T. Zhang, L. Hong, Y. Wang, Y. Xu, K. Ma, C. An, C. He, Z. Wei, F. Gao, J. Hou, *Adv. Mater.* **2020**, *32*, 1908205.

[18] W. Gao, H. Fu, Y. Li, F. Lin, R. Sun, Z. Wu, X. Wu, C. Zhong, J. Min, J. Luo, H. Y. Woo, Z. Zhu, A. K. Y. Jen, *Adv. Energy Mater.* **2021**, 2003177.

[19] L. Liu, Y. Kan, K. Gao, J. Wang, M. Zhao, H. Chen, C. Zhao, T. Jiu, A. K. Jen, Y. Li, *Adv. Mater.* **2020**, *32*, 1907604.

[20] H. N. Tran, S. Park, F. T. A. Wibowo, N. V. Krishna, J. H. Kang, J. H. Seo, H. Nguyen-Phu, S. Y. Jang, S. Cho, *Adv. Sci.* **2020**, *7*, 2002395.

[21] T. Wang, R. Sun, M. Shi, F. Pan, Z. Hu, F. Huang, Y. Li, J. Min, *Adv. Energy Mater.* **2020**, *10*, 2000590.

[22] Z. Luo, R. Ma, T. Liu, J. Yu, Y. Xiao, R. Sun, G. Xie, J. Yuan, Y. Chen, K. Chen, G. Chai, H. Sun, J. Min, J. Zhang, Y. Zou, C. Yang, X. Lu, F. Gao, H. Yan, *Joule* **2020** *4*, 1236.

[23] J. Wu, G. Li, J. Fang, X. Guo, L. Zhu, B. Guo, Y. Wang, G. Zhang, L. Arunagiri, F. Liu, H. Yan, M. Zhang, Y. Li, *Nat. Commun.* **2020**, *11*, 4612.

[24] J. Yao, B. Qiu, Z. G. Zhang, L. Xue, R. Wang, C. Zhang, S. Chen, Q. Zhou, C. Sun, C. Yang, M. Xiao, L. Meng, Y. Li, *Nat. Commun.* **2020**, *11*, 2726.

[25] C. Zhu, J. Yuan, F. Cai, L. Meng, H. Zhang, H. Chen, J. Li, B. Qiu, H. Peng, S. Chen, Y. Hu, C. Yang, F. Gao, Y. Zou, Y. Li, *Energy Environ. Sci.* **2020**, *13*, 2459.

[26] M. Zhang, L. Zhu, G. Zhou, T. Hao, F. J. N. C. Liu, *Nat. Commun.* **2021**, *12*, 309.

[27] M. Zeng, X. Wang, R. Ma, W. Zhu, Y. Li, Z. Chen, J. Zhou, W. Li, T. Liu, Z. He, H. Yan, F. Huang, Y. Cao. *Adv. Energy Mater*. **2020**, *10,* 2000743.

[28] Z. Cao, J. Chen, S. Liu, X. Jiao, S. Ma, J. Zhao, Q. Li, Y. P. Cai, F. Huang, *ACS Appl. Mater. Interfaces* **2020**, *12*, 9545.

[29] P. Chao, H. Chen, Y. Zhu, N. Zheng, H. Meng, F. He, *Macromolecules* **2019**, *53*, 165.

[30] F. Liu, C. Xiao, G. Feng, C. Li, Y. Wu, E. Zhou, W. Li, *ACS Appl. Mater. Interfaces* **2020**, *12*, 6151.

[31] T. Liu, T. Yang, R. Ma, L. Zhan, Z. Luo, G. Zhang, Y. Li, K. Gao, Y. Xiao, J. Yu, X. Zou, H. Sun, M. Zhang, T. Pen˜, Z. Xing, H. Liu, X. Li, G. Li, J. Huang, C. Duan, K. Wong, X. Lu, X. Guo, F. Gao, H. Chen, F. Huang, Y. Li, Y. Li, Y. Cao, B. Tang, H. Yan, *Joule* **2021**, *5*, 1.

[32] R. Wang, J. Yuan, R. Wang, G. Han, T. Huang, W. Huang, J. Xue, H. C. Wang, C. Zhang, C. Zhu, P. Cheng, D. Meng, Y. Yi, K. H. Wei, Y. Zou, Y. Yang, *Adv. Mater.* **2019**, *31*, 1904215.

[33] C. Duan, L. Ding, *Sci. Bull.* **2020**, *65*, 1422.

[34] G. P. Kini, S. J. Jeon, D. K. Moon, *Adv. Mater.* **2020**, *32*, 1906175.

[35] J. Yang, P. Cong, L. Chen, X. Wang, J. Li, A. Tang, B. Zhang, Y. Geng, E. Zhou, *ACS Macro Lett.* **2019**, *8*, 743.

[36] H. Yao, J. Wang, Y. Xu, S. Zhang, J. Hou, *Acc. Chem. Res.* **2020**, *53*, 822.

[37] J. S. Park, G. U. Kim, D. Lee, S. Lee, B. Ma, S. Cho, B. J. Kim, *Adv. Funct. Mater.* **2020**, *30*, 2005787.

[38] H. Wang, T. Liu, J. Zhou, D. Mo, L. Han, H. Lai, H. Chen, N. Zheng, Y. Zhu, Z. Xie, F. He, *Adv. Sci.* **2020**, *7*, 1903784.

[39] Q. Zhang, M. A. Kelly, N. Bauer, W. You, *Acc. Chem. Res.* **2017**, *50*, 2401.

[40] T. Liu, Y. Zhang, Y. Shao, R. Ma, Z. Luo, Y. Xiao, T. Yang, X. Lu, Z. Yuan, H. Yan, Y. Chen, Y. Li, *Adv. Funct. Mater.* **2020**, *30*, 2000456.

[41] C. Duan, L. Ding, *Sci. Bull.* **2020**, *65*, 1597.

[42] C. Y. Liao, Y. Chen, C. C. Lee, G. Wang, A. J. J. Facchetti, *Joule* **2019**, *4*, 1.

[43] W. Li, K. H. Hendriks, W. S. C. Roelofs, Y. Kim, M. M. Wienk, R. A. J. Janssen, *Adv. Mater.* **2013**, *25*, 3182.

[44] W. Li, K. H. Hendriks, M. M. Wienk, R. A. J. Janssen, *Acc. Chem. Res*. **2016**, *49*, 78.

[45] L. Pan, T. Liu, J. Wang, L. Ye, Z. Luo, R. Ma, S. Pang, Y. Chen, H. Ade, H. Yan, C. Duan, F. Huang, Y. Cao, *Chem. Mater.* **2020**, *32*, 7309.

[46] X. Song, N. Gasparini, M. M. Nahid, S. H. K. Paleti, C. Li, W. Li, H. Ade, D. Baran, *Adv. Funct. Mater.* **2019**, *29*, 1902441.

[47] M. Shi, T. Wang, Y. Wu, R. Sun, W. Wang, J. Guo, Q. Wu, W. Yang, J. Min, *Adv. Energy Mater.* **2020**,*11*, 2002709.

[48] Z. Wang, J. Ji, W. Lin, Y. Yao, K. Zheng, Z. Liang, *Adv. Funct. Mater.* **2020**, *30*, 2001564.

[49] X. Liu, Y. Yan, A. Honarfar, Y. Yao, K. Zheng, Z. Liang, *Adv. Sci.* **2019**, *6*, 1802103.

[50] P. W. M. Blom, V. D. Mihailetchi, L. J. A. Koster, D. E. M. J. A. *Adv. Mater*. **2007**, *19*, 1551.

[51] Y. Gao, Z. Shen, F. Tan, G. Yue, R. Liu, Z. Wang, S. Qu, Z. Wang, W. Zhang, *Nano Energy* **2020**, *76*, 104964.

[52] K. Zhang, Z. Liu, N. Wang, *J. Power Sources* **2019**, *413*, 391.

[53] Z. Liang, J. Tong, H. Li, Y. Wang, N. Wang, J. Li, C. Yang, Y. Xia, *J. Mater. Chem. A* **2019**, *7*, 15841.

[54] S. R. Cowan, A. Roy, A. J. J. P. R. B. Heeger, *Phys. Rev. B: Condens. Matter* **2010**, *82*, 462.

[55] L. J. A. Koster, V. D. Mihailetchi, R. Ramaker, P. W. M. J. A. P. L. Blom, *Appl. Phys. Lett.* **2005**, *86*, 123509.

[56] B. Bernardo, D. Cheyns, B. Verreet, R. D. Schaller, B. P. Rand, N. C. Giebink, *Nat. Commun.* **2014**, *5*, 3245.

[57] C. L. Braun, *J. Chem. Phys.* 1**984**, *80*, 4157.

[58] K. Li, P. P. Khlyabich, L. Li, B. Burkhart, B. C. Thompson, J. C. Campbell, *J. Phys. Chem. C* **2013**, *117*, 6940.

[59] J. Ji, X. Wu, P. Deng, D. Zhou, D. Lai, H. Zhan, H. Chen, *J. Mater. Chem. C* **2019**, *7*, 10860.

[60] G. G. Malliaras, J. R. Salem, P. J. Brock, C. J. P. R. B. Scott, *Phys. Rev. B* **1998**, *581*, 10371.

A series of halogen-free polymer donors were developed by an incorporation of DPP unit into the paradigm PBDB-T backbone, which have markedly lower frontier molecular orbital levels and extended optical absorption. The optimal **P75** based device shows the best PCE of 10.28%. A slight addition of $PC_{71}BM$ into the blend is found to further generate finer phase-separated domains and thus further boost the efficiency up to 12.20%.

Keywords: halogen-free, polymer donor, diketopyrrolopyrrole, nonfullerene acceptor, organic solar cells

Jingjing Ji,[1] Jiaqi Xie,[1] Junhui Tang,[1] Kaibo Zheng,[2,3] and Ziqi Liang[1*]*

Developing Halogen-Free Polymer Donor for Efficient Nonfullerene Organic Solar Cells by Addition of Highly Electron-Deficient Diketopyrrolopyrrole Unit

TOC Image

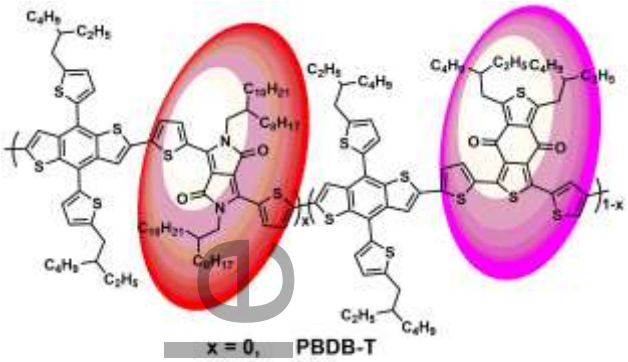

x = 0, PBDB-T
x = 1/4, P75
x = 1/2, P50
x = 3/4, P25
x = 1, P0